International Journal of Innovative Research in Computer Science & Technology (IJIRCST)
ISSN: 2347-5552, Volume-4, Issue-2, March, 2016

Investigation of SIDA Virus (HIV) Images Using Interferometry and Speckle Techniques

A.M. Hamed

***Abstract*- We investigate the SIDA virus images using two different techniques. Multiple beam modulated interference is considered since it gives contrasted images compared with two beam interference. The phase information of the image is extracted from the height depth. The second technique is based on speckle imaging of diffuser covered by the object information of SIDA image and compared with the ordinary subjective speckle image. Both speckle images are obstructed by uniform circular aperture. Discrimination between the two speckle images is attained as shown from the different plots.**

Keywords: **speckle imaging, processing of SIDA virus image, modulated multiple beam interference.**

I. INTRODUCTION

HIV is the Human Immunity deficiency Virus known as SIDA virus. This virus attacks the lymphatic immunity system. Transmission of HIV and other blood-borne viruses can occur during transfusion of blood components (i. e, whole blood, packed red cells, fresh-frozen plasma, cryoprecipitate, and platelets) derived from the blood of an infected individual. Depending on the production process used, blood products derived from pooled plasma can also transmit HIV and other viruses, but recombinant clotting factors cannot [1].

Tracking human immunodeficiency virus-type 1 (HIV-1) infection at the cellular level in tissue reservoirs investigated [2] provides opportunities to better understand the pathogenesis of infection and to rationally design and monitor therapy. Whole brain imaging of HIV – infected patients is presented [3] which is based on magnetization transfer ratio (MTR) histogram and fractional brain volume (FBV) measurements.

The reliable detection, sizing and sorting of viruses and nanoparticles is important for bio sensing, environmental monitoring, and quality control.

Manuscript Received March 20, 2016.

A.M. Hamed, Physics Department, Faculty of Science, Ain Shams University, Cairo 11556, Egypt

An optical detection scheme for the real-time and label-free detection and recognition of single viruses and larger proteins is introduced. The method makes use of Nanofluidic channels in combination with optical interferometry. Elastically scattered light from single viruses traversing a stationary laser focus is detected with a differential heterodyne interferometer and the resulting signal allows single viruses to be characterized individually [4, 5]. Recently, Discrimination between the normal and diseased stomach using speckle imaging is outlined [6]. Image processing of Corona Virus is investigated in recent publication based on interferometer and speckle techniques [7]. The modulated speckle imaging was investigated recently by the author [8- 13] and others [14, 15] and the applications of optical speckle imaging is outlined earlier in [16].

The image processing of HIV virus based on interferometer modulation and speckle imaging is investigated. The purpose of this study is based on the extraction of density information from the fringe shift which is related to the refractive index. In addition, discrimination between the speckle images in presence of the image and in its absence is outlined. Theoretical analysis is presented followed by computational results and discussion and finally conclusion is given.

II. THEORETICAL ANALYSIS

The complex amplitude of the SIDA virus as an object can be represented as follows:

$$A_{obj}(x, y; z) = a \exp[i\,\Phi(x, y; z)] \qquad (1)$$

Where a -is the amplitude of the image, and $\Phi(x, y; z)$ is its phase for an object at depth z. Equation (1) can be written in a discrete matrix form as follows:

$$A_{obj}(x, y; z) = \sum_{n=1}^{N}\sum_{m=1}^{M} a \exp\left[i\,\Phi(n\Delta x, m\Delta y; z)\right] \qquad (2)$$

Where a square matrix of dimensions N × N= 512× 512 pixels where N = M.

The 1st interferometric technique focuses on phase evaluation of the image using the phase shifting method. Coherent addition of a reference laser beam, $A_r = R \exp[i\,\Psi(x, y)]$ to the above object beam is considered to fabricate the modeled interference pattern. The laser beam is spatially filtered using a pinhole located in the focal plane of a converging lens in order to get uniform illumination. In this case, a plane wave is obtained. The pinhole pass only the central peak from the whole diffraction pattern and suppress all the diffraction legs and then the converging lens which is placed a distance (f) from the pinhole passes parallel rays of uniform intensity which is considered as a plane wave.

Then the intensity of the two beam interference obtained in the detector plane can be expressed as the modulus square as follows:

$$I = I_0\{1 + M\cos[\Phi(x, y; z) - \Psi(x, y)]\} \quad (3)$$

Where I(x, y; z) is the intensity of the modulated interference field at the point $I(x, y)$ for object depth z, $I_0 = |R|^2 + |a|^2$, is the function that characterizes the mean intensity of the interference pattern and $M = (2a\,R)/[|R|^2 + |a|^2]$, is the function that determines the modulation of the interference signal. In this case, the obtained trigonometric function has straight line fringes modulated by the object phase information. The modulated intensity is rewritten in matrix form as follows:

$$I = I_0 \sum_{n=1}^{N} \sum_{m=1}^{M} \{1 + M\cos[\Phi(n\Delta x, m\Delta y; z) - \Psi(n\Delta x, m\Delta y)]\} \quad (4)$$

Certainly, the d. c term in equation (3), $I_0 = |a|^2 + R^2$.
R is the amplitude of the coherent laser beam and that Ψappeared in equation (3) its phase. The equation (4) is used in the fabrication of the phase-shifted images outlined in equation (5).

Since the distance between any two fringes = λ/2. Consequently, according to the phase shift technique [7, 9], the phase information of the image is governed by the following equation:

$$\Psi(n\Delta x, m\Delta y) = \Phi(n\Delta x, m\Delta y; z) - \tan^{-1}\left[\frac{I_3(x, y) - I_2(x, y)}{I_1(x, y) - I_2(x, y)}\right] \quad (5)$$

Where the range of the interference phase $\Phi(n\Delta x, m\Delta y)$ extends from 0 up to 2π for a height z, I_1 is the intensity given in equation (4) at a phase $\Psi = \pi/2$, I_2 has $\Psi = \pi$, and I_3 has phase $\Psi = 3\pi/2$. Then, three equations are solved to get equation (5).

Once the phase is determined across the interference field, the corresponding height distribution h(x, y) on the surface of coronavirus can be determined [2] as follows:

$$h(x, y; z) = \frac{\lambda}{4\pi}\Phi(n\Delta x, m\Delta y; z) \quad (6)$$

We have assumed the surface measured at normal incidence. Almost all interferometers used to measure surface height variations use phase-shifting techniques.
The refractive index of the image of SIDA virus (μ) is computed as follows:
Since the phase of the wave cumulates traveling a distance L in a medium is

$$\Phi(x, y; z) = \int_L k\,dl = \int \frac{\mu(x, y, z)\,\omega}{c}\,dl \quad (7)$$

Then, the same wave that propagates over two equivalent paths L in SIDA virus medium and in vacuum gives the phase difference as follows:

$$\Delta\Phi(x, y; z) = \int (k - k_0)\,dl = \int [\mu(x, y, z) - 1]\frac{\omega}{c}\,dl \quad (8)$$

Where $k = \omega/c = 2\pi/\lambda$ is the propagation wave number in a medium of refractive index μ while k_0 is the propagation constant in vacuum.
By differentiation w.r.t. the path l= z, the refractive index distribution of the SIDA virus image is computed as follows:

$$\mu(x, y) = 1 + \frac{c}{\omega}\frac{d}{dz}[\Delta\Phi(x, y; z)] \quad (9)$$

Since the angular frequency is related to the wavelength as $\omega = 2\pi c/\lambda$ and $\Delta\Phi(x, y) = (\frac{2\pi}{\lambda})(O.P.D.)$ then the above equation becomes:

$$\mu(x, y) = 1 + \frac{d}{dz}[O.P.D.] \quad (10)$$

The optical path difference represents the height variation of the image, namely h (x, y, z) then equation (10) becomes:

$$\mu(x,y) = 1 + \frac{d}{dz}[h(x,y,z)] \quad (11)$$

The differentiation of the height distribution h(x, y, z) with respect to z give the differential fringe shift and the amplitude of the planar image a(x, y). Consequently, we finally get equation (12).

$$\mu(x,y)_{const.x} = 1 + a(x,y)\frac{\delta z}{\Delta z} \quad (12)$$

The fringe shift is δz with respect to inter-fringe spacing Δz at constant x, the fringes are assumed located in the x-y plane and z is the axis normal to the fringe system which represents the height depth and a (x, y) represents the amplitude of the image. In equation (12), h (x, y, z) = a (x, y). δz.

A. Computation of the Contrast

Consider the visibility expression to represent the fringe contrast as follows:

$C = \frac{I_{max} - I_{min}}{I_{max} + I_{min}}$. Substitute in equation (3), we get this result for the contrast:

$C=M=2R/(1+R^2)$ (13)

While the contrast given in case of multiple beam interference is extracted from the transmitted intensity distribution:

$$I_t = \frac{I_0}{1 + F\,sin^2[\Phi(x,y) - \Psi(x,y)]/2} \quad (14)$$

The parameter $F = 4R/(1-R)^2$ and the corresponding contrast is given by the formula (11). The maximum and minimum intensities are obtained from equation (13) as:

$I_{max} = I_0$ for $[\Phi(x,y) - \Psi(x,y)] = 2m\pi$, m is integer.

$I_{min} = I_0 / (1 + F)$ for $[\Phi(x,y) - \Psi(x,y)] = m\pi$

It is known that the refractive index has a direct relation with the polychromatic spectral distribution of illuminating light according to the Cauchy formula as follows:

$$\mu_\lambda = a + b/\lambda^2$$

Where a, and b are constants. Then the fringe shift and the refractive index are affected by the change of the wavelength.

III. COMPUTATIONAL RESULTS AND DISCUSSION

A gray scale image of SIDA virus of dimensions 512× 512 pixels is plotted as shown in the figure (1). The profile of the image of SIDA virus at horizontal line at 256 pixels is plotted as in the figure (2). The image has dimensions of 512 × 512 pixels.

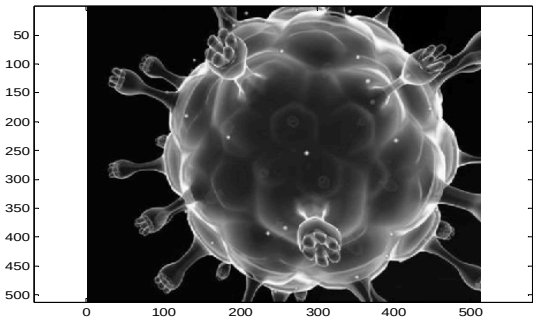

Figure (1): SIDA image of dimensions 512× 512 pixels.

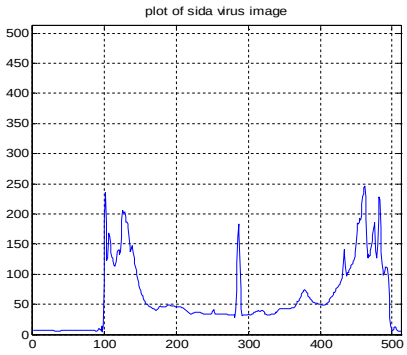

Figure (2): Plot of the image of SIDA virus at horizontal line at 256 pixels. The image has dimensions of 512 × 512 pixels

The SIDA virus image is processed using two different techniques of multiple beam interferometry modulated by the investigated image and speckle photography technique. The multiple beam interference of 32 fringes is plotted as in the figure (3). The two border fringes are apparent for the magnified photo. It is known that the resolution of multiple beam interference is better than two beam interference. Hence, the processing of the image using multiple beam interference is recommended.

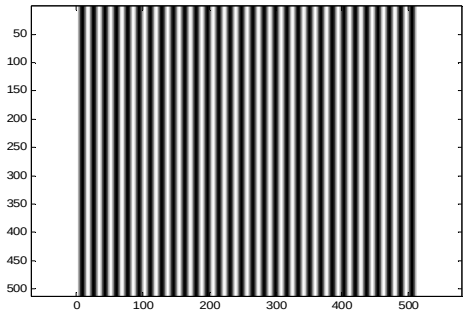

Figure (3): Multiple beam interference used in the processing of SIDA virus.

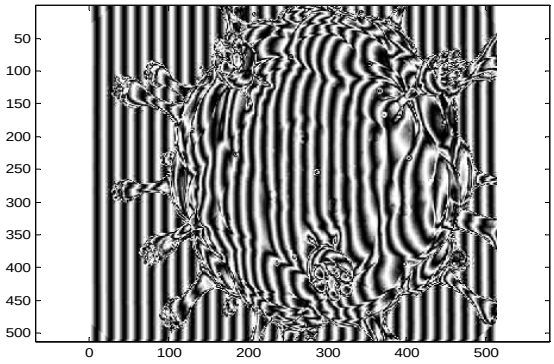

Figure (4- a): Modulated interference fringes with the SIDA virus image.

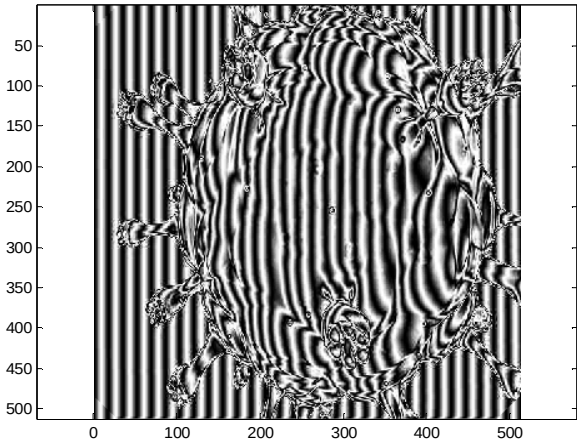

Figure (4- b): Modulated interference fringes with the SIDA virus image.

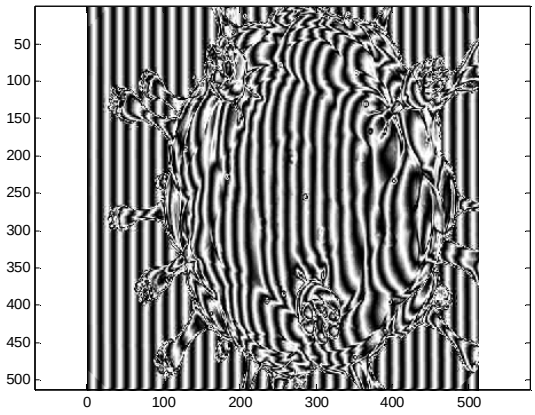

Figure (4- c): Modulated interference fringes with the SIDA virus image.

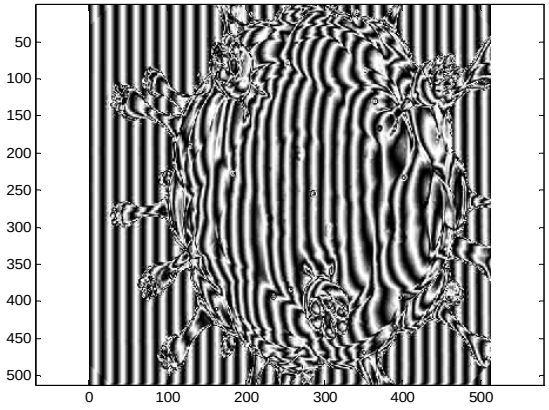

Figure (4- d): Modulated interference fringes with the SIDA virus image.

The technique of formation of modulated interference by the SIDA virus image used Mat- Lab code giving the image presented in the figure (4- a). The Mat- Lab code is the following:

```
F = 4*r1^2*(sin(y/0.5 - (1/32)* A (i, j)) ^2);
Intensity (i, j) = 1/ ((1-r1^2) + F);
```

The phase shifting technique is applied to get the phase of the image substituting in equation (5) in the analysis, where the results of the phase shifting method are summarized as shown in the figures (4 a- d). The phase image of the SIDA virus image derived from the interference shift images shown in the figure (3 a- d) is represented in the figure (5).

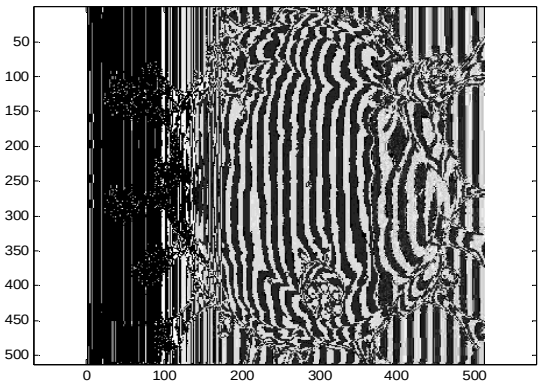

Figure (5): The phase image of the SIDA virus image derived from the interferometric images shown in the figure (4 a- d).

Table (1): The refractive index values as a function of the Z coordinate at certain horizontal line at 150 pixels. ΔZ = 34 pixels the inter-fringe spacing. The shift of the modulated fringes is towards the left

Z	Z_{image}	$\delta Z = Z - Z_{image}$	$\mu(Z) = 1 + \delta Z/\Delta Z$
172	151	21	1.62
206	177	29	1.85
240	221	19	1.65
274	251	23	1.68
308	287	21	1.62
342	324	18	1..53
376	356	10	1.29
410	396	14	1.41

Table (2): The refractive index values as a function of the Z coordinate at certain horizontal line at 200 pixels. ΔZ = 34 pixels the inter-fringe spacing. The shift of the modulated fringes is towards the left

Z	Z_{image}	$\delta Z = Z - Z_{image}$	$\mu(Z) = 1 + \delta Z/\Delta Z$
172	157	15	1.44
206	191	15	1.44
240	218	22	1.65
274	251	23	1.68
308	285	23	1.68
342	320	22	1..65
376	358	18	1.53
410	389	21	1.62

Table (3): The refractive index values as a function of the Z coordinate at certain horizontal line at 250 pixels. ΔZ = 34 pixels the inter-fringe spacing. The shift of the modulated fringes is towards the left

Z	Z_{image}	$\delta Z = Z - Z_{image}$	$\mu(Z) = 1 + \delta Z/\Delta Z$
172	157	15	1.44
206	187	19	1.56
240	218	22	1.65
274	250	24	1.71
308	286	22	1.65
342	317	25	1..73
376	359	17	1.50
410	396	14	1.41

Table (4): The refractive index values as a function of the Z coordinate at certain horizontal line at 300 pixels. ΔZ = 34 pixels the inter-fringe spacing. The shift of the modulated fringes is towards the left

Z	Z_{image}	$\delta Z = Z - Z_{image}$	$\mu(Z) = 1 + \delta Z/\Delta Z$
172	161	11	1.32
206	183	23	1.68
240	219	21	1.62
274	251	23	1.68
308	285	23	1.68
342	320	22	1..65
376	365	11	1.32
410	394	16	1.47

Table (5): The refractive index values as a function of the Z coordinate at certain horizontal line at 350 pixels. ΔZ = 34 pixels the inter-fringe spacing. The shift of the modulated fringes is towards the left

Z	Z_{image}	$\delta Z = Z - Z_{image}$	$\mu(Z) = 1 + \delta Z/\Delta Z$
172	164	8	1.24
206	195	11	1.32
240	230	10	1.29
274	256	18	1.53
308	305	3	1.09
342	329	13	1..38
376	368	8	1.24
410	394	6	1.18

Table (6): The refractive index values as a function of the Z coordinate at certain horizontal line at 400 pixels. ΔZ = 34 pixels the inter-fringe spacing. The shift of the modulated fringes is towards the left

Z	Z_{image}	$\delta Z = Z - Z_{image}$	$\mu(Z) = 1 + \delta Z/\Delta Z$
172	163	9	1.44
206	197	9	1.44
240	216	24	1.65
274	251	23	1.68
308	279	29	1.68
342	339	3	1..65
376	376	0	1.53
410	416	6	1.62

The values of refractive index extracted from the figure (6) using equation (12) are given from the fringe shift of the modulated image as in the figure (6). The profiles at 150, 200, and 250 pixels, are shown as in the Figure (7- a), while the profiles at 300, 350, and 400 pixels are plotted as in the figure (7- b). The profile peaks of the shifted fringes are used in the computation of the refractive index.

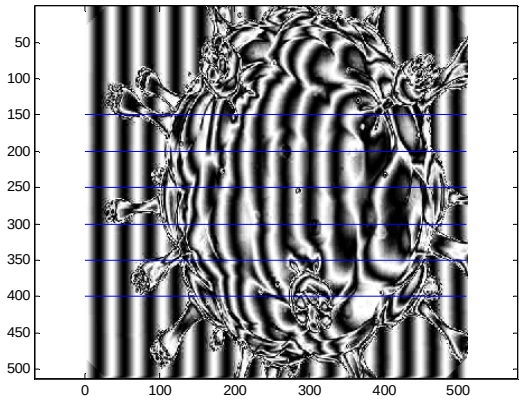

Figure (6)

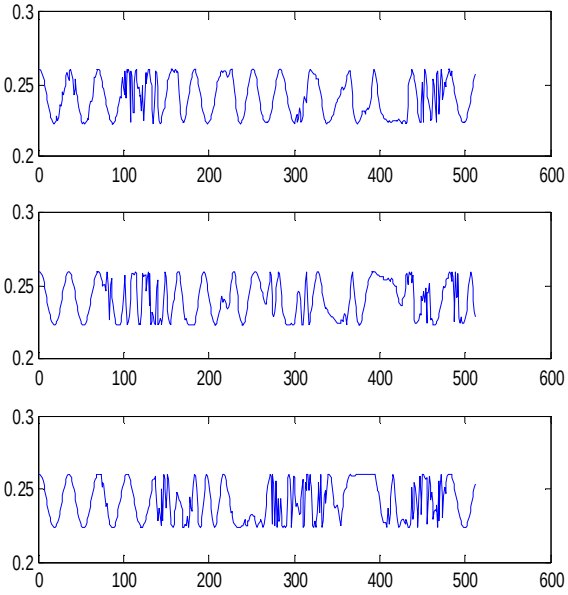

Figure (7- a): Three different profiles at 150, 200, and 250 pixels, where delta z = 34 pixels

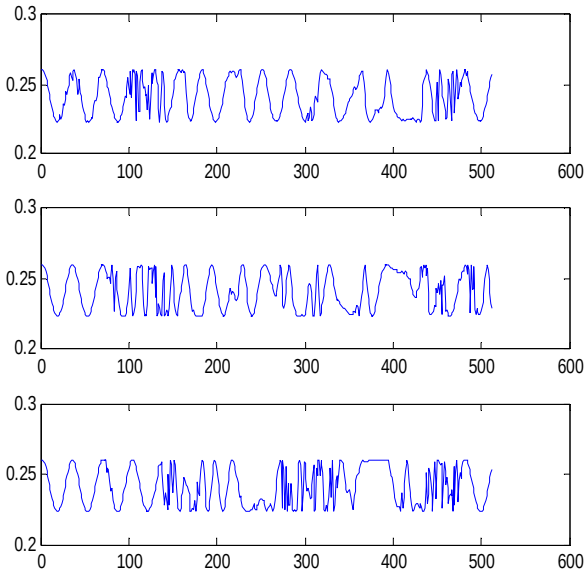

Figure (7- b): Three different profiles at 300, 350, and 400 pixels, where delta z = 34 pixels

The refractive index curves at three different horizontal lines at 150, 200, and 250 pixels are plotted as shown in the figure (8). The continuous blue curve corresponds to the refractive index at horizontal line at 150 pixels, discontinuous red curve at 200 pixels, while the green discontinuous curve at 250 pixels. It is shown that the

curves oscillate at the borders of the image showing greater values of the fringe shift hence greater values of refractive index.

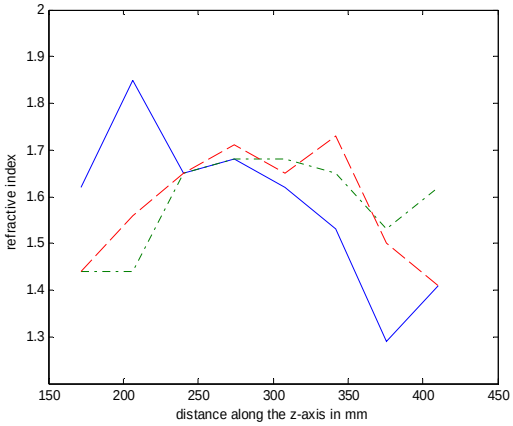

Figure (8): The continuous blue curve correspond to the refractive index at horizontal line at 150 pixels, discontinuous red curve at 200 pixels, while the green discontinuous curve at 250 pixels

The second technique of speckle imaging using the SIDA virus is based on the computation of the FFT algorithm of the multiplication of three functions. The 1st is the SIDA image, the 2nd is the obstructed circular aperture, and the 3rd is the diffuser function. Consequently, the obtained speckle image is the convolution product of the FFT of each function as shown in the plot of Figure (9).

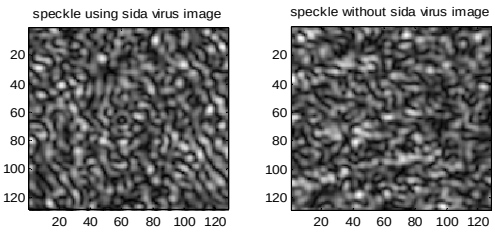

Figure (9): In the left, the speckle image using diffuser modulated by the SIDA virus image and obstructed by circular aperture, while in the right the ordinary speckle image in absence of the image is shown

In the left, the speckle image using diffuser modulated by the SIDA virus image and obstructed by circular aperture, while in the right the ordinary speckle image in absence of the image is shown. Discrimination between the two speckle images is observed comparing the two images. Quantitatively, we observe the difference between the two speckle images by comparing the two plots at certain horizontal line. Three plots at horizontal lines at 32, 64, and 96 pixels are shown as in the figure (10 a- c). The circular aperture of diameter =128 pixels is considered in the processing of all images.

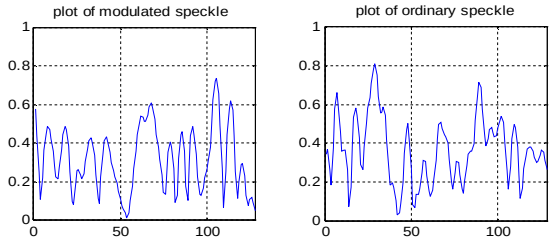

Figure (10- a): Plot of the modulated speckle by the SIDA virus image and the ordinary speckle obtained in absence of the SIDA virus image. Both of the speckle images used the same diffuser and obstructed by circular aperture of diameter = 128 pixels. The two plots are taken at horizontal line at 32 pixels.

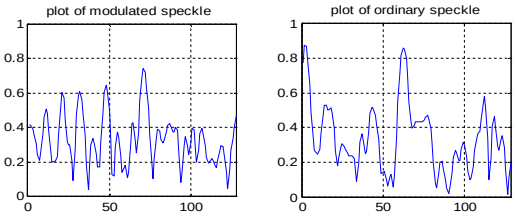

Figure (10- b): Plot of the modulated speckle image and the ordinary speckle obtained in absence of the SIDA virus image. The two plots are taken at horizontal line at 64 pixels

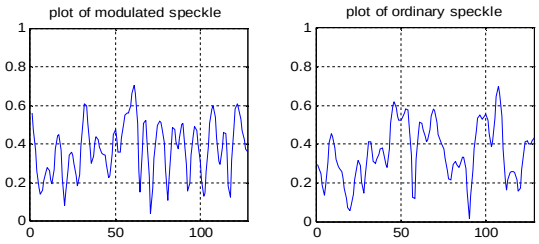

Figure (10- c): Plot of the modulated speckle image and the ordinary speckle obtained in absence of the SIDA virus image. The two plots are taken at horizontal line at 96 pixels.

IV. CONCLUSION

Firstly, the refractive index distribution is computed for the image of SIDA virus making use of the fringe shift occurred in the interference image. For the virus legs the fringe shift has greater values than the core and this may be attributed to the strong penetration of the nervous lymphatic cells.

Secondly, speckle imaging of the SIDA virus is compared with the ordinary speckle images using certain diffuser in both cases. This speckle coding is considered useful for discrimination from any other speckle image.

REFERENCES

[1] Elizabeth Donegan , MD, University of California San Francisco, HIV In Site Knowledge - Base Chapter October (2003).

[2] A.T. Haase , K. Henry, M. Zupancic , G. Sedgewick, R.A. Faust ,H. Melroe ,W. Cavert ,K. Gebhard, K. Staskus , Z.Q. Zhang, P.J. Dailey, H.H.Jr. Balfour , A. E rice , A.S. PerelsonScience , 274 (1996) 985-989.

[3] Ge. Yulin, L. K. Dennis, S.B. James, J.M. Lois, and I.G. Robert, AJNR Am J Neuroradiology 87(2003) 82–87.

[4] T. Plakhotnik , V. Palm . Interferometric Signatures of Single Molecules. Phys. Rev. Lett.87 (2001) 183602.

[5] J.S. Batchelder, D.M. DeCain, M.A.Taubenblatt, H.K. Wickramasinghe, C.C. Williams. Particulate Inspection of Fluids Using Interferometric Light Measurements. U S Patent (1991) 5,061,070.

[6] A.M. Hamed, Intern. J. of Innovative Res. in Eng. & Management (IJIREM), 3(2016)125- 133.

[7] A.M. Hamed, Opt. and Photonics J. (under processing).

[8] A.M. Hamed, J. Modern Opt 56 (2009) 1174- 1181.

[9] A.M. Hamed, J. Modern Opt. 56 (2009) 1633- 1642.

[10] A.M. Hamed, J. Opt. Eng. 50 (2011) 1- 7

[11] A.M. Hamed, Optics and Photonics Journal 1 (2011) 41.

[12] A.M. Hamed, Precision Instrument and Mechanology 3 (2014) 144- 152.

[13] A.M. Hamed, Topics on optical and digital image processing using holography and speckle techniques, publisher Lulu.com, ISBN 9781329328464 Nov. 29, 2015.

[14] Martha Lucía Molina Prado, Néstor Bolognini, and MyrianTebaldi, Opt. Comm. 338(2015)473- 478.

[15]E. Mossoa, M. Tebaldia, A.Lencinaa, N.Bolognini, Opt. Comm. 283(2010)1285- 1290.

[16]M. Francon, Laser speckle and applications in optics, Academic press, New York, 1979.

